

# Degradation of phenol by visible light assisted electrocatalytic treatment using N-V co-doped TiO<sub>2</sub> as photocatalyst and response surface methodology

Fuchen Ban\*, Huadong Nan, Qiu Jin, Yanxin Wang

School of Municipal and Environmental Engineering, Shenyang Jianzhu University, Shenyang 110168, China

\*E-mail: [1203951930@qq.com](mailto:1203951930@qq.com)

Received: 4 November 2020/ Accepted: 12 March 2021 / Published: 30 April 2021

---

In this study, simulated phenolic wastewater was treated by visible-light-assisted electrocatalysis using  $\gamma$ -Al<sub>2</sub>O<sub>3</sub>-supported N-V co-doped TiO<sub>2</sub> nanocatalysts as particle electrodes. The Box-Behnken design response surface method was utilized to study the factors affecting the degradation of phenol wastewater by visible light assisted electrocatalytic treatment and the interaction between these factors. The influence of the factors on the phenol removal rate decreases in the following order: pH > distance between electrodes > electrolyte concentration. The influence of the interaction among the factors on the phenol removal rate decreases in the following order: pH and electrolyte concentration > pH and distance between electrodes > distance between electrodes and electrolyte concentration. The optimized conditions are as follows: a phenol concentration of 180 mg/L, a COD of 387.5 mg/L, a pH of 2.82, a distance between electrodes of 11.00 cm and an electrolyte concentration of 0.96 mg/L, corresponding to an optimal COD removal rate of 81.86%. Visible-light-assisted multiphase electrocatalysis has an outstanding effect on the treatment of simulated phenolic wastewater.

---

**Keywords:** Response Surface Methodology; Visible light; Photoelectricity; Phenol

## 1. INTRODUCTION

Phenol is a chemical that is widely used as a raw material in industry. Phenol is used in the production or manufacture of such products as explosives, coatings, synthetic resins, pharmaceuticals, and phenolic plastics. Phenol is also used in petroleum, tannery pesticides, dyes, and other industries [1-2]. Phenolic wastewater accumulates easily in the environment and is harmful to human health [3-4]. Conventional coagulation, flocculation, precipitation, adsorption, and other removal methods only result in phenol transfer. Problems of secondary pollution and poor adaptability to changes in the sewage concentration remain [5]. In recent years, the use of electrochemical oxidation for phenol removal has been increasingly studied, but this method has the disadvantages of a high catalytic energy consumption, a high treatment cost and a low current efficiency [6]. A novel method has been developed in which

photocatalysis is combined with traditional electrochemical oxidation to treat wastewater. You and others [7-10] treated organic wastewater by combining photoelectric technology with particle electrodes and electrode plates with photocatalytic properties with outstanding results. Xu and others [11] fixed a silver phosphate photocatalyst with strong visible-light catalytic activity to an electrode surface to form a novel Ti/IrO<sub>2</sub>-Pt photoelectrode with considerable development potential. Metal-oxide-semiconductor (e.g., TiO<sub>2</sub>, SnO<sub>x</sub> and ZnO) photocatalysts are only active under ultraviolet light. As ultraviolet light accounts for only 5% of sunlight, the visible-light response of photocatalysts have been studied to fully exploit sunlight [12]. A N-V/TiO<sub>2</sub>/γ-Al<sub>2</sub>O<sub>3</sub> particle electrode was prepared in this study. The utilization of visible light by the electrode is improved by TiO<sub>2</sub> N-V co-doping. The phenol concentration was correlated with the electrode plate spacing, the initial pH and the electrolyte concentration using the Box-Behnken design response surface method, with the COD removal rates as indices. The technological conditions for the removal of phenol from wastewater by a visible light assisted electrocatalytic process were optimized to provide a theoretical basis for the engineering application of the technology.

## 2. MATERIALS AND METHODS

### 2.1. Materials

Phenolic wastewater was simulated in this study. The wastewater was prepared by adding specific reagents at concentrations of 150 mg/L. Analytical standards of phenol, 4-aminoantipyrine, concentrated sulfuric acid, absolute ethyl alcohol, anhydrous sodium sulfate, carbamide and tetrabutyl titanate were purchased from Liaoning Chemical Industry Co., Ltd., Xilong Chemical Co., Ltd. and the Development Center for Chemical Reagents in Tianjin. Glacial acetic acid was obtained from the Chemical Reagent Co., Ltd.

The following instruments were used for testing: a 350-W short-arc xenon lamp; a 881-6 thermostatic blast dryer; a JD5000-2 electronic balance; a YJ65 DC power supply; a 750 W-30 L air compressor; an LZB-3 WB rotor flowmeter; a 752 UV-Vis spectrophotometer; a LC-DMS-PRON magnetic stirrer and a SX2-2.5-10N muffle furnace.

### 2.2. Methods

Determination of COD<sub>Cr</sub>. Rapid closed catalytic digestion was used to determine the COD<sub>Cr</sub>. Standard solutions were made up at concentrations of 50, 100, 200, 400, 600, 800 and 1000 mg/L. A volume of 3 ml of each standard solution was placed in a heating tube (for a total of 6 tubes) to which 1 ml of a masking agent was added. Next, 3 ml of the digestion solution and 5 ml of the catalysts were added to the tube, mixed well and sealed. The heating tube was placed in a blast dryer, and the reaction was allowed to proceed for 15 min after a temperature of 165°C was reached; the tube was then removed and allowed to cool; next, 3 ml of distilled water were added to the tube; the tube was then shaken, and the absorbance of the solution was measured against a blank reagent at 600 nm. The obtained curve is shown in Figure 1.

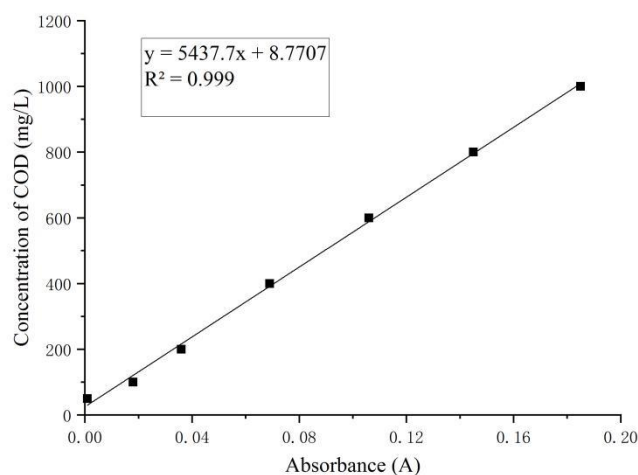


**Figure 1.** CODcr standard curve

The CODcr removal rate in the experiment was calculated as follows:

$$\eta = \frac{C_0 - C_t}{C_0} \times 100\% \quad (2-2).$$

In the equation above,  $\eta$  is the COD removal rate, and  $C_0$  and  $C_t$  are the degraded CODcr measured at times 0 and t, respectively (mg/L).

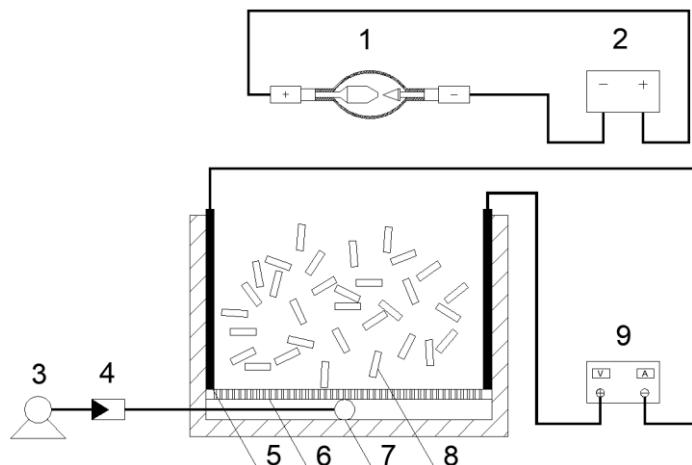
Preparation of N-V/TiO<sub>2</sub>/γ-Al<sub>2</sub>O<sub>3</sub> particle electrodes. A prescribed quantity of butyl titanate was mixed with anhydrous ethanol; the resulting solution was mixed with glacial acetic acid, double steamed water, and anhydrous ethanol under strong stirring to produce titania sols. The sols were calcined for 3 h at 400°C in a muffle furnace to produce a pure nano TiO<sub>2</sub> powder. A series of N-V/TiO<sub>2</sub> products with different vanadium contents (Moore percentages, see below) was obtained by adding urea (Co(NH<sub>2</sub>)<sub>2</sub>) as a nitrogen source and ammonium metavanadate (NH<sub>4</sub>VO<sub>3</sub>) as a vanadium source to the obtained powder, where the N doping was fixed at a 20% molar percentage. The γ-Al<sub>2</sub>O<sub>3</sub> carrier was pretreated with dilute acid before being doped with different quantities of the powder. The carrier was impregnated with N-V/TiO<sub>2</sub> powder in a constant-temperature water bath pot and dried overnight in a 70°C drying box followed by roasting for 3 h in a muffle furnace at 400°C. Catalysts were prepared using commercial pure titanium dioxide Degussa P-25 (P25) for comparison with the novel catalyst.

An experiment was performed using a 350-W short-arc xenon lamp as a visible light source. The effective processing volume of the electrolytic reactor was 14 cm × 12 cm × 10 cm. The effective oxidation area of the electrode plate was 10 cm × 10 cm. A Ru-IrO<sub>2</sub>/Ti polar plate was used as the anode, where the plate oxide coating has a long life, a high electrocatalytic activity, and resistance to electrical contact friction. The cathode was titanium plate, and the particle electrode was placed in the reactor.

The electrode plates were pretreated using the following procedure. The cathode and anode plates were soaked in dilute hydrochloric acid solution for 12 h and subsequently washed with distilled water until impurities on the plates were removed. Next, the plates were soaked in distilled water for 12 h and dried at 110°C.

The pre-treated electrode plates were installed at both ends of the reactor and the self-fabricated particle electrode was placed in the reactor. The simulated phenolic wastewater was added to the reactor

followed by prescribed quantities of  $\text{Na}_2\text{SO}_4$  electrolyte and an acid-base reagent. An air compressor was turned on to aerate the reactor, where the aeration volume was controlled by a rotor flow meter. A cooling fan and a xenon lamp were turned on, and the DC-regulated power supply was adjusted to output a prescribed voltage. The reaction solution was sampled every 10 min up to 60 min. The experimental device is shown in Figure 2.



1-Short arc Xenon lamp, 2-Xenon lamp power supply, 3-Air compressor, 4-Rotor flowmeter, 5-electrolytic plate, 6-Aeration plate, 7-Aeration plate inlet, 8-particle electrode, and 9-regulated power supply

**Figure 2.** Schematic of the experimental device.

### 3. RESULTS AND DISCUSSION

#### 3.1. Catalyst characterization

Figure 3 (a) shows the UV-Vis absorption curve for  $\text{N-V/TiO}_2/\gamma\text{-Al}_2\text{O}_3$ . The light absorption intensity of the  $\text{N-V/TiO}_2/\gamma\text{-Al}_2\text{O}_3$  particle electrode has been extended to the range of visible light response, showing that N-V the co-doping has successfully increased the absorption and utilization of visible light by the particle electrode. The absorption intensity increases with the V ratio.

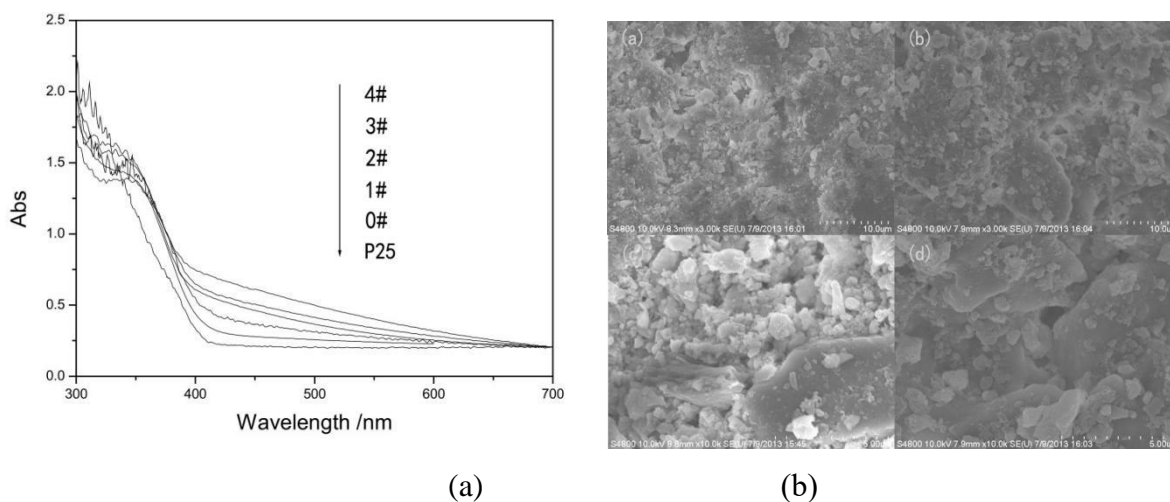


**Figure 3.** UV-visible light absorption curves of N-V/TiO<sub>2</sub>/ $\gamma$ -Al<sub>2</sub>O<sub>3</sub> (a) and SEM images of various catalysts (b) (a and c are electron micrographs of  $\gamma$ -Al<sub>2</sub>O<sub>3</sub> at 3000x and 10000x magnifications, respectively; b and d are electron micrographs of N-V/TiO<sub>2</sub>/ $\gamma$ -Al<sub>2</sub>O<sub>3</sub> at 3000x and 10000x magnifications, respectively).

Figure 3 (b) shows a SEM image of the catalyst. Compared with the  $\gamma$ -Al<sub>2</sub>O<sub>3</sub> carrier without loaded N-V/TiO<sub>2</sub> (panels a and c), there are fewer surface voids, which makes the surface more smooth: this change in the  $\gamma$ -Al<sub>2</sub>O<sub>3</sub> surface results from enhanced N-V/TiO<sub>2</sub> crystallization. The supported active components (Fig. b and d) provide the catalyst N-V/TiO<sub>2</sub>/ $\gamma$ -Al<sub>2</sub>O<sub>3</sub> with a stable crystal structure, a large specific surface area, and surface roughness, which meet the requirements for the catalyst.

### 3.2. Effect of pH

The reaction conditions were controlled as follows: the phenol concentration was 180 mg/L, the COD concentration was 387.5 mg/L, the distance between electrodes was 10 cm, the slot voltage was 25 V, the aeration rate was 9 L/min, the particle electrode dosage was 35 g/L, the Na<sub>2</sub>SO<sub>4</sub> electrolyte concentration was 1 g/L, and the reaction time was 30 min. The reaction was allowed to proceed under short-arc xenon lamp irradiation for 60 min. Fig. 4 shows the effect of the pH on the COD removal rate.

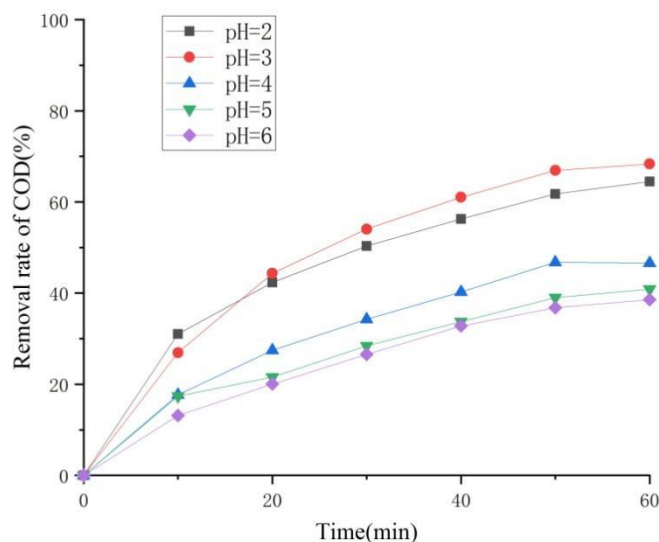
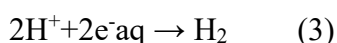
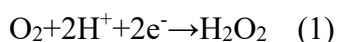


**Figure 4.** COD removal efficiency of MG (387.5mg/L) at (a) varying initial pH (initial concentration—387.5 mg/L, N-V/TiO<sub>2</sub>/γ-Al<sub>2</sub>O<sub>3</sub> particle electrode dosage—35g/L, voltage—25V, aeration—9L/min, distance between electrodes—10cm)

The visible-light-assisted electrocatalytic system produced a high COD removal rate over pH values ranging from 2.0 to 6.0. The highest of COD removal rate was 68.35% at pH 3.0. The acidity and alkalinity of the solution considerably affect the oxygen reduction reaction. In an acidic solution, oxygen undergoes a reduction reaction to form strongly oxidizing H<sub>2</sub>O<sub>2</sub> (formula 1), and the number of H<sub>2</sub>O<sub>2</sub> molecules generated also controls the number of hydroxyl radicals generated in the subsequent reaction (formula 2 is provided as an example).

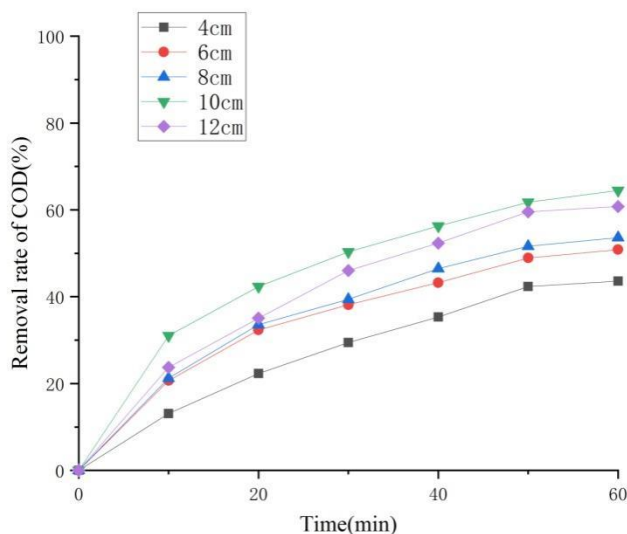


The lower the pH is, the higher the H<sup>+</sup> concentration is, and the more intense the hydrogen evolution in side reaction (3) is, which significantly affects the formation of ·OH and H<sub>2</sub>O<sub>2</sub>; the higher the pH is, the lower the H<sup>+</sup> concentration is, which can become sufficiently low to prevent reaction (1) from proceeding. However, a high pH inhibits H<sub>2</sub>O<sub>2</sub> decomposition. Zambrano [13] reported a relatively high removal rate of phenol and chemical oxygen demand under low pH conditions (pH 3 and 5). Acidic conditions can inhibit the oxygen evolution reaction, increasing the current efficiency and reducing energy consumption.

### 3.3. Effect of distance between electrodes

The reaction conditions were controlled as follows: the phenol concentration was 150 mg/L, the COD concentration was 387.5 mg/L, the pH was 2, the slot voltage was 25 V, the aeration rate was 9 L/min, the particle electrode dosage was 35 g/L, the Na<sub>2</sub>SO<sub>4</sub> electrolyte concentration was 1 g/L, and

the reaction time was 30 min. The reaction was allowed to proceed under short-arc xenon lamp irradiation for 60 min. The relationship between the electrode plate spacing and the phenol removal rate is shown in Figure 5.



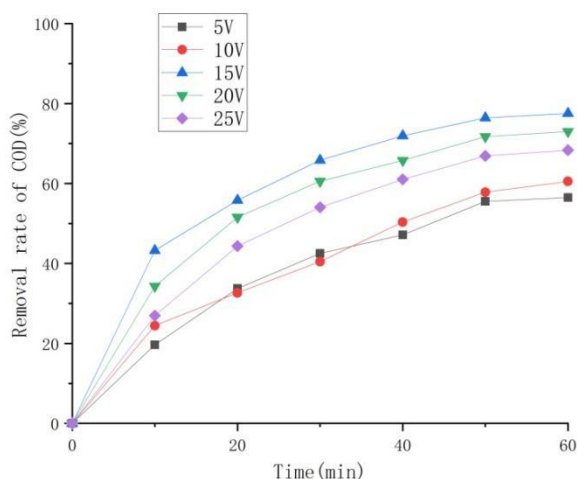
**Figure 5.** COD removal efficiency of MG (387.5mg/L) at (a) varying initial distance between electrodes (initial concentration—387.5 mg/L, N-V/TiO<sub>2</sub>/γ-Al<sub>2</sub>O<sub>3</sub> particle electrode dosage—35g/L, voltage —25V, aeration—9L/min, pH—2)

Fig. 5 shows that when the distance between electrodes increases from 4 cm to 10 cm, the removal rate increases. The COD removal rate is 64.47% at a 10-cm distance between electrodes: the resistance of the reactor increases with the distance between electrodes, and the number of polarized particle electrodes increases. Therefore, the removal rate increases. However, a further increase in the plate spacing to 12 cm clearly causes the removal rate to decrease. At a constant voltage, increasing the distance between electrodes inevitably causes the resistance of the entire system to increase, which decreases the electric field intensity of the reactor, indirectly increases the mass transfer distance, and slows the migration rate of organic molecules. Thus, the treatment becomes less effective [14]. Thus, 10 cm was chosen as the optimal distance between electrodes based on the experimental results.

### 3.4. Effect of slot voltage

Figure 6 shows the effect of the voltage on the COD removal rate. Increasing the voltage from 5 V to 15 V increases the removal rate to 77.54%. Increasing the voltage expands the potential difference between the conductive particles and the electrolyte, thus enhancing the driving force for electrochemical catalytic oxidation reaction and promoting the effective separation of photo-generated electron-hole pairs. Therefore, the number of photo-generated holes and hydroxyl radicals increases, and the photocatalytic efficiency increases with the current density. Increasing the voltage to 25 V causes the removal

rate to decrease to 68.35%. This result is obtained because increasing the voltage intensifies the side reaction: as a fixed quantity of photo-generated electrons are produced in a given time, the increased voltage limits the transfer of photo-generated electrons. The optimal voltage is chosen to be 15 V based on the analysis presented above. I. Aliet [15] obtained the optimum phenol degradation using a photoelectrocatalytic method at a 0.5-V external bias, and the degradation rate was 5.2 times faster than that obtained using undoped TiO<sub>2</sub> nanotubes.



**Figure 6.** COD removal efficiency of MG (387.5mg/L) at (a) varying initial slot voltage (initial concentration—387.5 mg/L, N-V/TiO<sub>2</sub>/γ-Al<sub>2</sub>O<sub>3</sub> particle electrode dosage—35g/L, distance between electrodes—10cm, aeration—9L/min, pH—2)

### 3.5. Effect of aeration

Figure 7 shows the effect of the aeration rate on the COD removal rate. The removal rate increased from 63.76% to 83.35%, as the aeration rate was increased from 7 L/min to 11 L/min.

This result is obtained because aeration produces a large number of ·OH, which considerably enhances the reaction efficiency. Increasing the aeration rate to 15 L/min considerably decreases the treatment efficiency for phenol. This result is obtained because excessive aeration indirectly increases the contact probability of particle electrodes, which increases the short circuit current and affects the removal efficiency. Thus, the aeration rate should be controlled at the optimum value of 11 L/min.

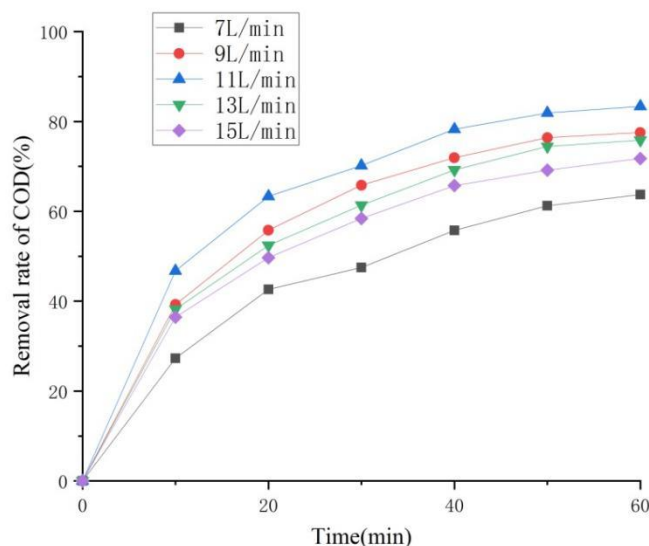


**Figure 7.** COD removal efficiency of MG (387.5mg/L) at (a) varying initial aeration (initial concentration—387.5 mg/L, N-V/TiO<sub>2</sub>/γ-Al<sub>2</sub>O<sub>3</sub> particle electrode dosage—35g/L, distance between electrodes—10cm, voltage —25V, pH—2)

### 3.6. Effect of supporting electrolyte concentration

In the visible-light-assisted electrocatalytic system, the conductivity efficiency in the reaction system is generally improved by adding suitable electrolytes to improve the removal of organic matter. Commonly used electrolytes are H<sub>2</sub>SO<sub>4</sub>, NaOH, KOH, Na<sub>2</sub>SO<sub>4</sub> and NaCl. The experimental results presented above show that visible light assisted electrocatalytic treatment is effective under acidic conditions; thus, Na<sub>2</sub>SO<sub>4</sub> or NaCl would be suitable as reference electrolytes under the acidic conditions used in this study. However, refractory halides are easily produced in electrochemical reactions in which NaCl is used as the electrolyte [16], whereas Na<sub>2</sub>SO<sub>4</sub> is relatively stable and does not affect the test results. Hence, Na<sub>2</sub>SO<sub>4</sub> was used as the electrolyte in this study.

The reaction conditions were controlled as follows: the phenol concentration was 150 mg/L, the COD concentration was 387.5 mg/L, the pH was 3, the distance between electrodes was 10 cm, the slot voltage was 15 V, the aeration rate was 9 L/min, the particle electrode dosage was 35 g/L, and the reaction time was 30 min. The reaction was allowed to proceed under short-arc xenon lamp irradiation for 60 min. The relationship between the electrode plate spacing and the phenol removal rate is shown in Figure 8.

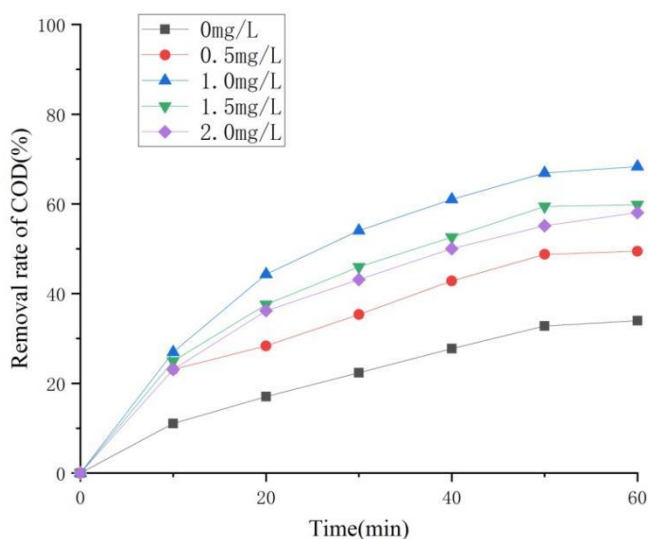


**Figure 8.** COD removal efficiency of MG (387.5mg/L) at (a) varying initial electrolyte concentration (initial concentration—387.5 mg/L, N-V/TiO<sub>2</sub>/γ-Al<sub>2</sub>O<sub>3</sub> particle electrode dosage—35g/L, distance between electrodes—10cm, voltage —15V, pH—3, aeration—9L/min)

Figure 8 shows that when the electrolyte concentration increases to 1 g/L, the COD removal rate gradually increases. This result is obtained because the addition of electrolytes can effectively increase the conductivity of the reaction solution and facilitate the formation of strong oxides, such as  $\cdot\text{OH}$  and  $\text{H}_2\text{O}_2$ . When the electrolyte concentration is increased above the optimal value of 1 g/L, the removal rate decreases. Increasing the electrolyte concentration to 2 g/L results in a COD removal rate of only 58.06%, which is 10.29 lower than that at 1 g/L. This result is obtained because an excessive number of electrolyte molecules can cause the solution conductivity to increase continuously. The resulting intense side reactions increase the energy consumption and are often accompanied by bubbles, which affect phenol removal. Therefore, 1 g/L was selected as the optimal  $\text{Na}_2\text{SO}_4$  concentration in this study.

### 3.7. Design and Results

The three factors that affect the treatment effect of wastewater, i.e., the pH, the distance between electrodes and the electrolyte concentration, were chosen as variables X1, X2 and X3, respectively. The response value was the phenol removal rate. The Box-Behnken design model was implemented using Design-Expert 10.0.1 software as a 3-factor 3-level experiment. The range of factors was determined using a single factor test. The design factor codes and levels are shown in Table 1. The experimental design and results for the response surface are shown in Table 2. Other authors have performed a similar number of experiments using BBD. For example, Dalvand and others [17] performed a total of 27 runs using four parameters for the simultaneous analysis of PAHs and BTEX in soil; Garg [18] performed 17 experimental runs using three parameters to observe *Pseudomonas putida* with a reactive dye.

**Table 1.** Design Factor Coding and Level Experimental design.

Factors	Variable	Level		
		-1	0	1
pH	X <sub>1</sub>	2	3	4
Distance between electrodes (cm)	X <sub>2</sub>	9	10	11
Electrolyte concentration (g/L)	X <sub>3</sub>	0.8	1.0	1.2

**Table 2.** Experimental Design and Results of Response Surface

Number	pH	Distance between electrodes (cm)	Electrolyte concentration (g/L)	COD removal rate (%)
1	3	10	1	83.65
2	3	10	1	83.68
3	4	9	1	72.37
4	3	10	1	83.66
5	4	10	1.2	68.83
6	3	11	0.8	79.52
7	3	9	0.8	82.46
8	4	10	0.8	69.72
9	4	11	1	69.13
10	3	9	1.2	82.33
11	2	9	1	75.84
12	3	10	1	83.64
13	2	10	0.8	76.11
14	3	10	1	83.63
15	3	11	1.2	78.46
16	2	11	1	75.34
17	2	10	1.2	73.15

The variance analysis results for the regression model and the COD removal rate obtained using Design-Expert software are shown in Tables 3 and 4. The multivariate quadratic regression equation between the factors and the response values obtained from the data analysis is given below:

$$Y=83.68-2.55X_1-1.32X_2-0.63X_3-0.69X_1X_2+0.52X_1X_3-0.23X_2X_3-9.63X_1^2-0.89X_2^2-2.10X_3^2 \quad (3-1)$$

Table 3 shows that the correlation coefficient R<sup>2</sup> of the model is 0.9956, and the experimental error is small; Radj2R<sup>2</sup> is 0.9900, and Rpred2R<sup>2</sup> is 0.9332; that is, the difference between the correction coefficient and the prediction coefficient is only 5.68%, which indicates that the model prediction fits the experimental results well [19].

**Table 3.** ANOVA results of regression models

Std. Dev	0.56	R-Squared	0.9956
Mean	77.74	Adj R-Squared	0.9900
C.V. %	0.72	Pred R-Squared	0.9332
PRESS	35.12	Adeq PreCision	35.070

Table 4 shows that the F value of the model is 177.52 and that the model is significant. The F value shows that the influence of the three factors on the removal of phenol from wastewater decreases in the following order: pH > distance between electrodes > electrolyte concentration, where the model P is less than 0.0001. Thus, the model can reliably predict the treatment effect of wastewater.

**Table 4.** ANOVA results of COD removal rate

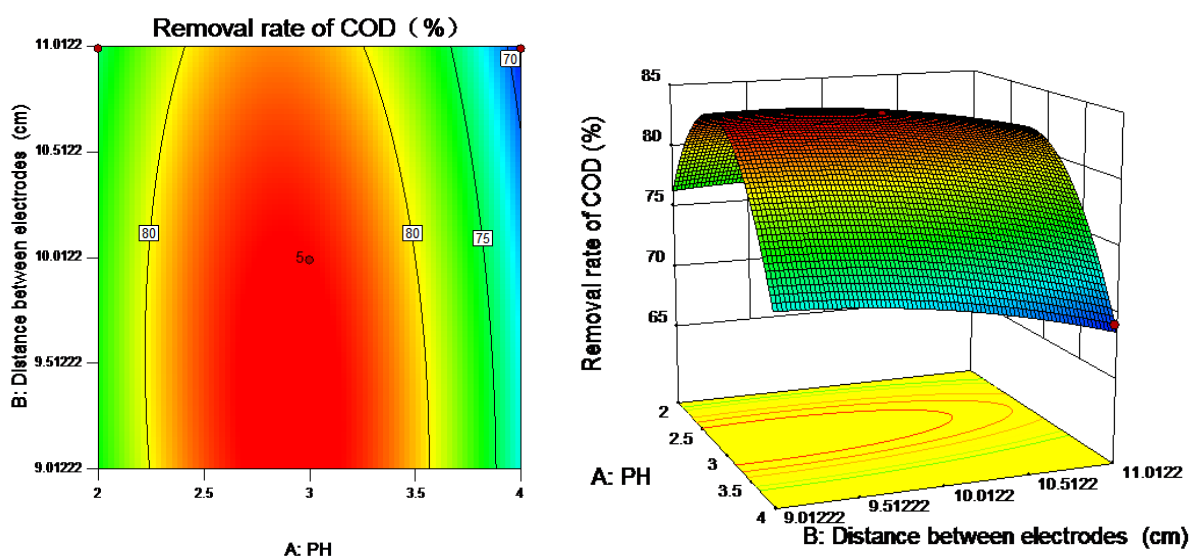
Project	Total variances	Degree of freedom	F	P	-
Model	501.03	9	177.52	< 0.0001	significant
X <sub>1</sub>	51.97	1	165.72	< 0.0001	
X <sub>2</sub>	13.91	1	44.37	0.0003	
X <sub>3</sub>	3.18	1	10.13	0.0154	
X <sub>1</sub> X <sub>2</sub>	1.88	1	5.99	0.0443	
X <sub>1</sub> X <sub>3</sub>	1.07	1	3.42	0.1070	
X <sub>2</sub> X <sub>3</sub>	0.22	1	0.69	0.4337	
X <sub>1</sub> <sup>2</sup>	390.07	1	1243.85	< 0.0001	
X <sub>2</sub> <sup>2</sup>	3.30	1	10.52	0.0142	
X <sub>3</sub> <sup>2</sup>	18.61	1	59.35	0.0001	
Residual	2.20	7			
Lack of Fit	2.20	3			
Pure Error	0.000	4			
Cor Total	503.22	16			

### 3.8. Two-factor interaction effect analysis

The contours and response surfaces for the interactions between the three factors affecting the removal efficiency of COD from wastewater are shown in Figure 9 to Figure 11. In the contour map, the central elliptical contour shows that the interaction between the two factors is significant, and the central circle indicates that the interaction between the two factors is weak; the steep slope of the response surface indicates that the response value is highly sensitive to the two factors.

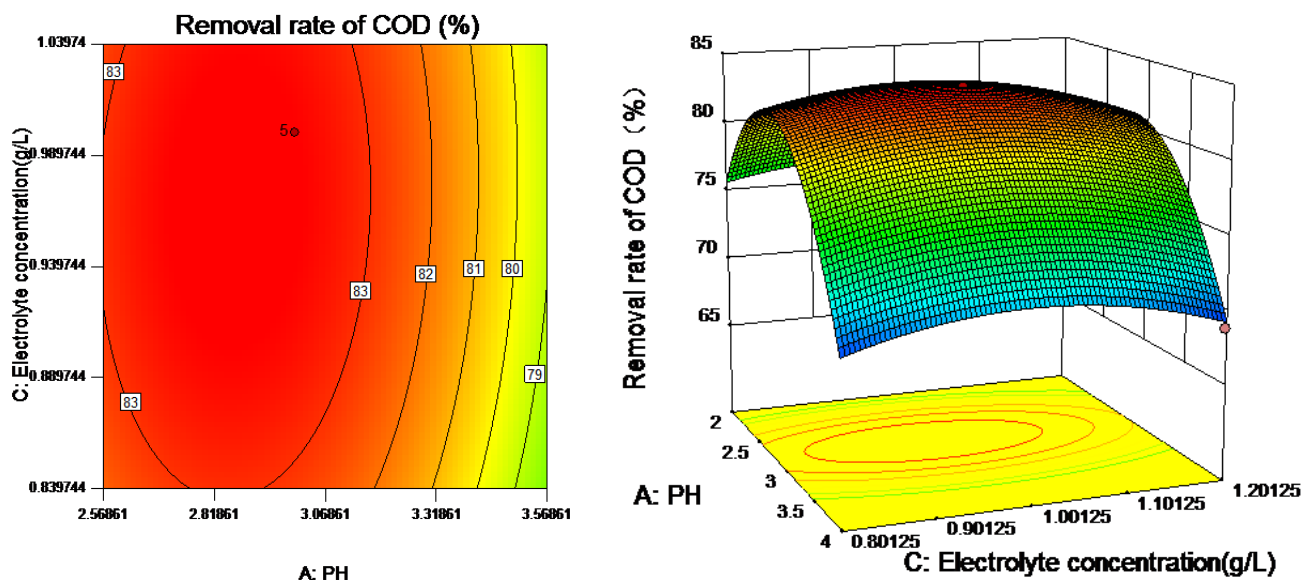
Figure 9 shows how the interaction between the pH and the distance between electrodes affects the COD removal rate. The contour map is elliptical, that is, the interaction between the two factors is significant. As the pH increases, the COD removal rate first increases and then decreases, and the same

trend is observed for varying the distance between electrodes. The response surface diagram shows that the COD removal rate is sensitive to changes in the two factors, where the effect of pH is stronger than that of the distance between electrodes. The removal rate reaches a maximum of 83.68% at a pH of 3 and a distance between electrodes of approximately 10 cm. Increasing the pH further reduces the side reactions that produce hydrogen and increases the  $\cdot\text{OH}$  and  $\text{H}_2\text{O}_2$  concentration. The results of Wang and others [20] suggest that the removal efficiency of COD and total organic carbon is high under acidic conditions because the decomposition of hydroxyl radicals and oxygen evolution is inhibited. Increasing the distance between electrodes increases the number of polarized particle electrodes, which accelerates the degradation of phenol. Decreasing the pH and the distance between electrodes gradually reduces the mass transfer efficiency, which lowers the removal rate.



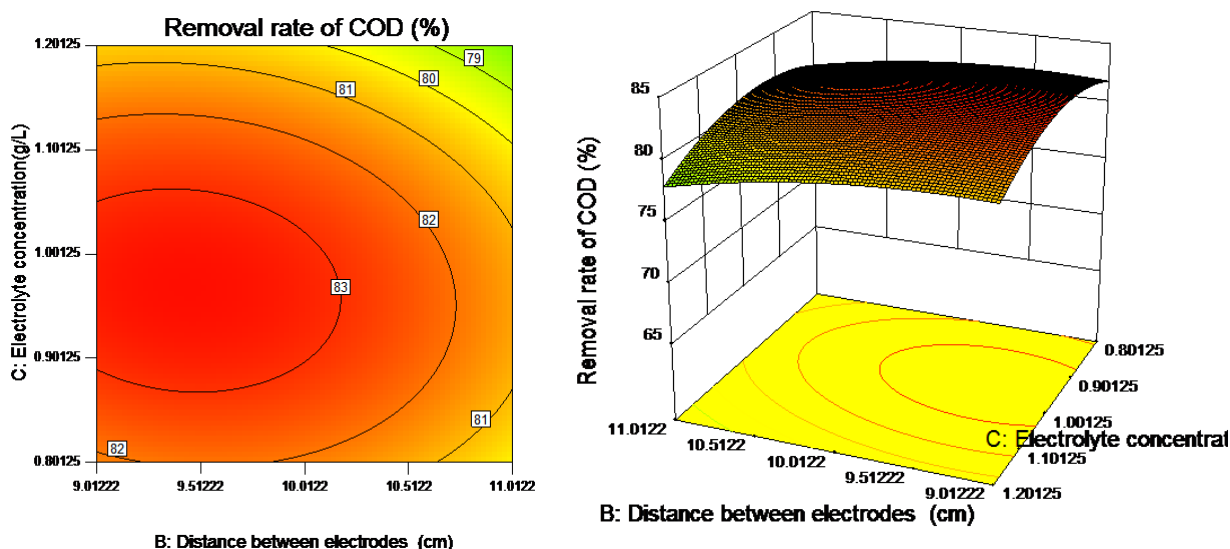
**Figure 9.** Contour and response surface of interaction between pH and distance between electrodes

Figure 10 shows how the interaction between the pH and the electrolyte concentration affects the COD removal rate. The contour diagram shows that the interaction between the two factors is significant, and the response surface diagram shows that the removal rate is highly sensitive to changes in the two factors, where the effect of the pH is stronger than that of the electrolyte concentration. Increasing the pH causes a gradual decrease in the removal rate: the COD removal rate is very high in the pH range of 2.5-3.5. The maximum removal rate of 81.85% is obtained at a pH of approximately 2.8 and an electrolyte concentration of approximately 1.0 g/L. As the electrolyte concentration and pH increase, the conductivity of the reaction solution increases, which promotes the formation of strong oxides, such as  $\cdot\text{OH}$  and  $\text{H}_2\text{O}_2$ , thereby accelerating COD removal. However, increasing the pH and the electrolyte concentration beyond the optimum values limits the COD removal rate because of the occurrence of side reactions and the reduction in the  $\text{H}^+$  concentration.



**Figure 10.** Contour and response surface of interaction between pH and electrolyte concentration

Figure 11 shows how the interaction between the distance between electrodes and the electrolyte concentration affects the COD removal rate. The contour map does not show a noticeable interaction between the two factors, that is, the interaction of the two factors has a relatively weak effect on the COD removal rate. The distance between electrodes has a stronger effect on the removal rate than the electrolyte concentration.



**Figure 11.** Contour and response surface of interaction between the distance between electrodes and electrolyte concentration

We can identify the following trend for the three independent variables of the pH, the distance between electrodes and electrolyte concentration from the results of the analysis presented above. The pH is the most influential factor followed by the distance between electrodes, and the electrolyte concentration is the least influential factor.

The above mentioned results from the Design-Expert software analysis show that the optimal response value Y is 81.86, that is, the maximum removal rate is 81.86%. The optimal values of the three main factors are a pH of 2.82, a distance between electrodes of 11.00 cm and an electrolyte concentration of 0.96 mg/L.

#### 4. CONCLUSIONS

A visible-light-assisted electrocatalytic method was used to treat simulated phenolic wastewater using a  $\gamma$ -Al<sub>2</sub>O<sub>3</sub>-supported N-V co-doped photocatalyst as a particle electrode. The N-V/TiO<sub>2</sub>/ $\gamma$ -Al<sub>2</sub>O<sub>3</sub> particle electrode exhibited good photocatalytic performance in the visible-light-assisted electrocatalytic system. This electrode had a good response to visible light. An optimization analysis of the Box-Behnken design response surface showed that the influence of various factors on the treatment effect of wastewater dyed with methyl orange and treated by the electrochemical method decreases as follows: pH > distance between electrodes > electrolyte concentration. A contour and response surface analysis showed the influence of the interaction between the factors on the treatment effect of wastewater decreases as follows: pH and electrolyte concentration > pH and distance between electrodes > distance between electrodes and electrolyte concentration. The optimal values of the three main influencing factors were found to be a pH of 2.82, a distance between electrodes of 11.00 cm and an electrolyte concentration of 0.96 mg/L, corresponding to an optimal removal rate of 81.86%. The model can be used to make reliable predictions for the treatment of phenolic wastewater.

#### ACKNOWLEDGMENTS

This work was financially supported by Liaoning Natural Science Fund Project (Z2415053)

#### References

1. X. Sun, C. Wang, Y. Li, W. Wang & J. Wei, *Desalination*, 355 (2015) 68-74.
2. J.Y. Liu, Y. Zhang, L. Zhang, L. Hua, G.P. Zeng, C.Z. Yang, *Industrial Water Treatment*, 38 (2018) 12~16.
3. P. Kazemi, M. Peydayesh, A. Bandegi, T. Mohammadi & O. Bakhtiari, *Chemical Engineering Research and Design*, 92 (2014) 375-383.
4. S. Mohammadi, A. Kargari, H. Sanaeepur, K. Abbassian, A. Najafi & E. Mofarrah, *Desalination and Water Treatment*, 53 (2015) 2215-2234.
5. L.G.C. Villegas, N. Mashhadi, M. Chen, D. Mukherjee, K.E. Taylor & N. Biswas, *Curr Pollution Rep*, 2 (2016) 157-167.
6. Y.J. Feng, X.Y. Li, *Water Research*, 37 (2013) 2399-2407.
7. H. You, Z. Wu, Y. Jia, X. Xu, Y. Xia, Z. Han & Y. Wang, *Chemosphere*, 183 (2017) 528-535.
8. Y.J. Deng, Y. Lu, J.K. Liu & X.H. Yang, *European Journal of Inorganic Chemistry*, 22 (2015) 3708-3714.
9. Z.D. Li, M. Li, J.W. Tang, *Chinese Journal of Environmental Engineering*, 6 (2019) 1-12.
10. Y.B. Zhang, S.H. Chen, *Nonferrous Metals Engineering*, 9 (2019) 93-98.
11. X. Guo, *Doctoral dissertation, CUG (Beijing)*, 2013.
12. X.D. Tang, Z.R. Wang, N. Liu, S.L. Liu, S.Y. Wu, *Technology of Water Treatment*, 46 (2020) 62-65.

13. J. Zambrano, P. Hyunwoong, and M. Booki, *Environmental Technology*, 41 (2019) 3248–3259.
14. D.H. Kim, M.A. Anderson, *Journal of Photochemistry and Photobiology A: Chemistry*, 94 (1996) 221-229.
15. I. Ali, S.R. Kim, S. P. Kim & J.O. Kim, *Catalysis Today*, 282 (2017) 31-37.
16. Z.Y. Yin, X.H. Li, Y.S. Hou, Z.J Yuan & X.X. Zheng, *Environmental Science & Technology*, 33 (2010) 150-153.
17. K. Dalvand & A. Ghiasvand, *Analytica Chimica Acta*, 1083 (2019) 119-129.
18. S.K. Garg, M. Tripathi and N. Lal, *Desalination and Water Treatment*, 54 (2014) 3122–3133.
19. S.C. Ferreira, R.E. Bruns, H.S. Ferreira, G.D.Matos, J.M. David, G.C. Brandao & W.N.L. Dos Santos, *Analytica Chimica Acta*, 597 (2007) 179-186.
20. Z. Wang, M. Xu, F. Wang, X. Liang, Y. Wei, Y. Hu & W. Fang, *Electrochimica Acta*, 247 (2017) 535-547.

© 2021 The Authors. Published by ESG ([www.electrochemsci.org](http://www.electrochemsci.org)). This article is an open access article distributed under the terms and conditions of the Creative Commons Attribution license (<http://creativecommons.org/licenses/by/4.0/>).